IGPP-UCR-72-2

A LARGE AREA DETECTOR FOR NEUTRONS BETWEEN 2 AND 100 MeV

R. T. Grannan, R. Koga, W. A. Millard, A. M. Preszler,
G. M. Simnett and R. S. White

Physics Department and
Institute of Geophysics and Planetary Physics
University of California
Riverside, California 92502

February 1, 1972

A Large Area Detector for Neutrons Between 2 and 100 MeV

R. T. Grannan, R. Koga, W. A. Millard, A. M. Preszler,

G. M. Simnett and R. S. White

Physics Department and
Institute of Geophysics and Planetary Physics
University of California
Riverside, California 92502

February 1, 1972

ABSTRACT

A neutron detector sensitive from 2 to 100 MeV is described. The detector is designed for high altitude balloon flight to measure the flux, energy and direction of albedo neutrons from the earth and to search for solar neutrons. A neutron scatter from a proton is required in each of two liquid scintillator tanks spaced 1 meter apart. The energy of the recoil proton in the first tank is obtained from pulse height analysis of the scintillator output. The energy of the recoil neutron is obtained from its time of flight between the tanks. The detector has been calibrated with 15.3 MeV neutrons and μ mesons. The minimum detectable flux is 10^{-4} neutron/cm^2-sec at a counting rate of one per minute, the energy resolution is 12% at 15 MeV and 30% at 100 MeV. The angle between the incoming neutron and the recoil neutron is measured to $\pm 10^{\circ}$.

1. INTRODUCTION

In order to understand the mechanisms for generating and accelerating particles in solar flares and for investigating their time behavior it is very useful to study the neutrons produced. If the temperature and the deuterium concentration in solar flares are sufficiently high, thermonuclear neutrons will be produced with high enough intensities to be observed near the earth.[1] In addition, neutrons will be generated by collisions of high energy solar flare protons with the helium atmosphere of the sun.[2,3] The solar neutron intensity at the earth will peak in the vicinity of 50 MeV. An identification of solar neutrons will give information about the density of helium and the flux of energetic protons in the sun's atmosphere, together with the time dependence of the protons' accelerations and losses. If energetic protons are stored for periods of time, the neutrons produced will give the proton time history.

The search for solar neutrons has been unsuccessful to date because of the low solar neutron flux and the limitations of the previously flown detectors. For a review of these attempts see Lockwood.[4] Above about 10 MeV the previous detectors have lowered the limit for the solar neutron flux to less than 10^{-2} neutrons/cm^2-sec. The detector described in this paper has the capability of measuring neutron fluxes down to 10^{-4} neutrons/cm^2-sec.

From the time of discovery of the high energy protons in the earth's radiation belt, their source was thought to be the decay of neutrons produced by nuclear interactions of cosmic ray

protons in the atmosphere of the earth. Our detector has the capability of measuring these albedo neutrons.

In order to search for solar neutrons and study earth albedo neutrons the detector requirements are 1) large area, solid angle, and efficiency; 2) energy determination capability in the interval from 2 to 100 MeV; and 3) high discrimination against backgrounds. Our detector was first proposed in 1968[5]. It utilizes the double scatter of a neutron from a proton in each of two liquid scintillator banks. The energy of the recoil proton is measured by pulse height analysis and the energy of the recoil neutron by the time of flight between the tanks.

The energy of the incoming neutron E_n is obtained from the sum of the energies of the recoil proton E_{p_1} and recoil neutron E_{n_1} as indicated in Figure 1a and equation (1):

$$E_n = E_{n_1} + E_{p_1} \tag{1}$$

The zenith angle θ, the angle between the incident neutron direction and the recoil direction is determined from

$$\tan \theta = \left(\frac{E_{p_1}}{E_{n_1}} \right)^{\frac{1}{2}} \tag{2}$$

If the direction P_1 were obtained, in addition, it would be possible to determine the azimuthal angle as well. The measurement of the direction of P_1 necessarily comes at the expense of a high detection efficiency. For our experiment the

compromise to a thick detector and therefore high efficiency was made. As a consequence, the direction of P_1 could not be measured.

In order to discriminate against backgrounds, a number of improvements were made over past detectors: 1) Liquid scintillator that has a large hydrogen to carbon ratio of 1.67 was used to reduce the number of neutron interactions on carbon. 2) Each liquid scintillator bank was completely surrounded by plastic scintillator to eliminate charged cosmic rays. 3) The mass of liquid scintillator was large, about 135 kg, a reasonable fraction of the total flight weight.

We thus have good energy resolution, a large area-solid angle-efficiency factor, and a good discrimination against background neutrons. Preliminary analysis of the data from a balloon flight launched on September 26, 1971 from Palestine, Texas gave several hundred thousand albedo neutrons in 20 hours of data. The backgrounds consist mostly of chance coincidence of neutrons and γ-rays between the two tanks and are less than a few percent of the neutrons. These results are reported elsewhere.[6]

2. THE NEUTRON DETECTOR

The detector is designed to operate at balloon altitudes where it efficiently discriminates against the large number of energetic charged particles. The size of the balloon limits the detector weight that can be carried to altitude and the charged particles restrict the overall dimensions. The detector

has an identical response to upward and downward moving neutrons so that solar and earth albedo neutrons may both be measured; this demands symmetry about a horizontal plane through the center of the detector. To make the detector more directional the position of the interactions of the incident and the scattered neutrons are each identified to about 10 cm. The trajectory of the scattered neutron is determined and the direction of the incident neutron is calculated to an accuracy of about 10%.

A schematic cross section of the neutron detector is shown in Figure 1b. The aluminum tanks, S_1 and S_2, are filled with liquid scintillator NE 223* (decaline). The tanks are 100 cm x 50 cm x 15 cm. They are mounted coplanar with a separation of 100 cm center to center. Each tank is optically separated into eight identical cells and each cell is viewed by a 5 in. Amperex XP 1040 photomultiplier tube. For optimum light collection the cell walls are painted white and each photomultiplier tube face is in contact with the liquid scintillator. A reservoir tank with both positive and negative pressure relief valves is attached to each of the main tanks to allow for thermal expansion and contraction of the liquid scintillator.

Extraneous material which might attenuate either the incident or scattered neutrons is avoided wherever possible. The walls of the tanks and the optical dividers are as thin as feasible structurally and the photomultipliers are mounted along

*Manufactured by Nuclear Enterprises, Ltd.,Winnipeg,Manitoba,Canada

two sides of the tanks, rather than on the top or bottom. The thickness of the top and bottom of the tank is 0.32 cm. The resultant dimension of the tank-photomultiplier tube assembly is 102 cm x 110 cm x 16 cm.

The overall dimensions of the detector are limited by the requirements placed on energy response, resolution and efficiency. The efficiency of the detector is determined by the areas and thicknesses of S_1 and S_2 and the solid angle subtended at one tank by the other. With the additional constraint on up/down symmetry, the optimum detector thickness is about 15 cm for neutron energies between 2 and 100 MeV. If it were thicker, there would be some increase in efficiency but multiple neutron scattering would degrade the angle measurement.

The area of the liquid scintillator tank is limited by the detector dead time. The fractional dead time was restricted to $\leq$ 1% to allow a safety margin for possible photomultiplier tube malfunction during a balloon flight. A secondary neutron of 2 MeV produced by the nuclear interaction of a cosmic ray in the detector has a maximum transit time of 55 nsec across the largest detector dimension. Thus it is prudent to disable the system for at least 70 nsec after a signal from the anticoincidence scintillator to give secondary neutrons time to escape. Each anticoincidence unit may be considered to have an area of 1.2 m^2 with a viewing solid angle of 4π ster. At high latitudes at solar minimum the counting rate will be $\approx 4 \times 10^4$ sec^{-1} in each anticoincidence system. With an allowance for photomultiplier tube noise equal to this, the dead time is 0.8%.

Charged particles are rejected by completely enclosing each liquid scintillator tank with a box of Pilot F* plastic scintillator, 6 mm thick. Each anticoincidence scintillator assembly has sheets 104 cm x 114 cm top and bottom, and four sheets interleaved to form the sides. The four side sheets are curved at the ends to produce overlap at the corners of the box. Each is viewed with a 2 in. photomultiplier tube (RCA 8575) via an adiabatic light guide. The corners of the "box" are rounded to reduce the maximum dimension of the detector. The top sheet of the anticoincidence scintillator box is viewed by two 5 in. photomultipliers (Amperex XP 1040) via adiabatic light guides, and the bottom sheet is viewed by two 2 in. photomultipliers (RCA 8575) via tapered light guides.

The scintillator box surrounding S_1 is referred to as A_1, with the designation A_{11}, A_{12} and A_{13} referring to the top, bottom and side sheets respectively (Figure 1). A similar notation is used for the components of the scintillator box A_2 surrounding S_2. A photograph of the assembled detector, showing the location of the anticoincidence sheets and light pipes, is given in Figure 2. One of the side scintillator sheets has been removed from the top assembly, exposing the liquid reservoir tank and four of the photomultiplier tubes that view the liquid scintillator.

The liquid scintillator tanks are supported at the corners by 2.5 cm square cross section, 6 mm wall thickness

*Manufactured by New England Nuclear,Corp.,Watertown,Mass.,USA

chrominum-molybdenum steel tubing visible in Figure 2. These strong support members are required for the 360 Kg detector to survive the parachute landing following a balloon flight. The tubing penetrates the lower sheet of the top anticoincidence shield (A_{12}) and the top sheet of the bottom anticoincidence shield (A_{21}). It is cut to a "U" cross section where it penetrates the scintillator to reduce the amount of scintillator removal. The frame is attached to the base of the aluminum gondola.

The gondola maintains the instrument at atmospheric pressure and near room temperature during a balloon flight. It has a 3.2 mm cylindrical wall and 1.6 mm spherical end caps. It is surrounded by 15 cm of expanded polystyrene. The total amount of material between the liquid scintillator and the outside atmosphere is 2 g cm^{-2} of which 0.75 g cm^{-2} is between the anticoincidence scintillator, A_{11}, and the atmosphere.

3. THE DETECTOR ELECTRONICS

For the detector to identify and measure the energy spectrum and angle of the neutrons, the electronics system must perform the following functions:

1. Reject charged particles and gamma rays.
2. Measure the energy of the recoil protons in S_1 and S_2.
3. Measure the time of flight of the scattered neutron between S_1 and S_2.
4. Record the cell or cells in which the complete event took place.
5. Measure the orientation of the detector with respect to the sun.

6. Switch the system response between a downward and an upward mode to enable both solar and albedo neutrons to be detected.

In addition, the telemetry must have the capacity to handle the expected counting rates.

A block diagram of the system electronics is shown in Figure 3. The anode pulses from the photomultiplier tubes of each detector tank are fed to an adder circuit where they are linearly summed. Prior to being summed, each photomultiplier tube line is connected to a cell identification circuit which consists of threshold discriminators, pulse stretchers and a shift register as a temporary memory. The pulses are summed in a linear passive array of transmission line transformers.

The summed signal goes to a 512 channel pulse height analyser (PHA) for amplitude analysis and a zero-walk discriminator to generate an accurate logic pulse to start the time of flight measurement. The PHA consists of a pulse amplifier-stretcher, a linear gate, a sample-and-hold circuit and an 8-bit analog to digital converter. The zero-walk circuit uses the constant fraction of pulse height technique to achieve a one-half nanosecond walk over a 100:1 dynamic range.[7,8]

Signals from the anticoincidence systems are summed and used to inhibit data processing. In addition, time of flight is used to discriminate against relativistic neutrons and gamma rays. The minimum acceptable time of flight is 5 nsec, the maximum time for a relativistic particle or proton to travel between S_1 and S_2 and the maximum time of flight is 70 nsec, the longest acceptable neutron time of flight.

With the occurrence of a valid event, i.e., threshold and time requirements satisfied and no anticoincidence signal, the input discriminators are inhibited. The PHA and time of flight circuits generate appropriate binary outputs that are encoded along with the cell identification and azimuthal information into a 128 bit, continuously transmitted telemetry frame. The frame consists of a 32 bit synchronization pattern and 96 bits of binary coded data telemetered to the ground via a PCM/FM carrier.

After reception and detection of the data by the ground receiver, the data clock signal is regenerated by the bit synchronizer. Four quadratic phases of the clock are produced and one is used to "clean" up the data stream as demodulated in the receiver. The data frame is synchronized by comparing 32 bits of the received bit stream with a 32 bit pre-programmed pattern and shifting the incoming data one bit/frame until there is agreement.

All data are displayed in binary form using neon lamps. In addition, all 23 data words are binary/decimal decoded and can be printed on paper tape for each valid event at the rate of one event/sec. The data is also converted from digital to analogue for display on spectrum analysers. Finally, the data bit stream is recorded on magnetic tape in an IBM compatible format.

All circuitry is constructed on double-sided copper clad epoxy board, with all the boards for the flight electronics on a common plane. Fast signals are routed using 2.1 mm semi-rigid 50 ohm cable. Fast logic circuitry consists of emitter coupled

logic (ECL) and Motorola MECL III series, while transistor transistor logic (TTL) is used elsewhere. Total power consumption from three packs of silver zinc cells is fifty-five watts.

4. SIGNAL ADDERS AND TIME OF FLIGHT CIRCUITRY.

Of the various circuits incorporated in the flight electronics, it is believed that the signal adder and time-of-flight circuits are of sufficient interest to merit further discussion.

A. THE SIGNAL ADDERS

The requirements of the signal adders are:

1. Summation of eight photomultiplier tube pulses;
2. Signal isolation input to input > 100:1 (40dB) to be able to identify a specific tube, and hence the cell;
3. Linear dynamic range > 100:1;
4. Rugged and lightweight.

The technique uses twisted wire pair transmission line transformers as illustrated in Figure 4. A section of the transformer configuration is shown in Figure 4a and the transmission line analogue in Figure 4b. The adder consists of an unbalanced-to-balanced transformer and a hybrid transformer. Isolation between the two inputs is dependent on the balance of the transformers and $R_R = R_L$. The advantage of the transmission line approach is that the interwinding capacitance, which limits the high frequency performance of transformers, combines smoothly with the series inductance of the line to produce wide band, resonance free operation.[9,10]

Transmission line length for the unbalanced-to-balanced transformer is relatively unimportant, as for any line correctly terminated in its characteristic impedance. With too short a line however, the amplitude response will fall off at low frequencies. This is caused by the decrease in the reactance of the equivalent transformer windings, this reactance being proportional to the length of the line. Since the permeability of ferrite falls at high frequencies, the electrical length of the line decreases to the physical length as the frequency increases. This is important when one examines the interconnection of the hybrid transformer. The output signal is the sum of the voltage at the input and output of the transmission lines. Therefore as the frequency increases greater amounts of phase difference occur, contributing to a fall-off in response. For this reason the length of the line should normally be $\lambda/8$ or less at the highest frequency of interest.

Adder sections are cascaded to achieve the summing of eight inputs together as shown in Figure 4c. The four wires needed for the two lines of the hybrids are twisted together to achieve a better balance before winding on the core. The hybrid at the input section has nine turns of No. 28 wire wound on the core whereas the output section requires 5 turns of No. 32 wire. For the unbalanced-to-balanced transformer, eleven turns of No. 32 wire are used in the input section and eleven turns of No. 28 wire on the output section. Ferronics 11-620-B or Indiana General CF-101/0-G cores with a μ = 5500, outside diameter of 5.85 mm, inside diameter of 3.05 mm and height = 1.52 mm were

used. Since the load impedance R_L is almost never purely resistive, the terminating impedance R_T, is composed generally of a parallel RLC so that the > 40 dB isolation can be met.

B. TIME OF FLIGHT CIRCUITRY

It is necessary to measure the times of 5 to 70 nsec with an uncertainty of less than one nsec. We use a time to voltage to binary conversion approach. A voltage proportional to the time of flight is generated, held and converted to an 8-bit binary output using a double ramp conversion technique. The time of flight circuit is shown in Figure 5. Preceding circuitry consists of a zero walk discriminator with ECL logic output levels.

Prior to an event, diodes D1 and D5 associated with the "START" and "STOP" signals are biased off. A 10mA constant current source establishes 5mA through each of diodes D2 and D3, so that there initially is no voltage on the sample and hold capacitor C1. A "START" signal activates the start circuitry diverting the 10mA current through D1. The 5mA current demanded by the 5mA current sink thus flows through capacitor C1. A linear negative ramp of about 6 mV/nsec is produced across C1. The ramp is terminated and the voltage held when "STOP" causes D5 to conduct. The stop circuitry now supplies the required current and reverse biases D4. Very fast switching transistors (Motorola MMT 3960A, with a current gain bandwidth product, f_T > 1.6 GHz and the MM4049, with f_T > 4 GHz) are used in a non-saturating mode together with hot carrier diodes in the input switching circuitry.

The capacitor voltage is buffered using a matched monolithic dual field effect transistor (FET), Q9. Local feedback is used to maintain the gate to source voltage, $V_{GS} = 0$. This results in only a few pico-amperes of gate bias current. The voltage is then amplified by a factor of 20 with a balanced differential amplifier IC4.

The amplified version of the capacitor voltage (VTOF) is converted to binary form by the dual ramp analog to digital converter. One must compare the amplified capacitor voltage with a stable reference voltage (VREF), developed across D8.[11] FET switch Q10 first connects the amplified capacitor voltage to integrator IC5. With the integrator output quiescently slightly negative, the application of the negative capacitor voltage causes a positive going ramp of slope V_{TOF}/RC volts per second, where RC are the components associated with integrator. Crossing zero, the output switches comparator IC6, allowing the 2 MHz clock pulses to fill registers IC8 and IC9.

After a fixed time the counter is filled, flip-flop IC10 switches and the integrator is switched to the positive reference voltage. The integrator output at a positive value proportional to V_{TOF} now becomes a negative-going ramp of V_{REF}/RC volts per second. The registers begin with a zero count when the reference voltage is switched in. When the integrator output crosses zero, clock pulses are inhibited. The stored count is then directly proportional to the value of the integrator output at the time of switchover and hence to the time-of-flight.

5. THE DETECTOR RESPONSE

The detector was calibrated by assigning the neutron recoil energies E_{n_1} from given times of flight and the proton recoil energies E_{p_1} from given pulse height analyzer voltage outputs. At low energies the detector was calibrated with 15.3 MeV neutrons produced by the Van de Graaff generator at the University of California at Riverside. At higher energies, E_{p_1} was deduced from the measured minimum ionizing cosmic ray μ-meson energy deposits. The overall efficiency was calculated from the known neutron cross-sections, composition and geometry of the detector.

For the time of flight calibration, measurements were made of the zero time, the channel number versus time and the time resolution. The zero time, the time of the origin of the pulse in the first neutron scatter, was obtained using γ-rays from inelastic neutron interactions on carbon in the liquid scintillator. Incoming neutrons interact in both S_1 and S_2 and the γ-rays produced travel forward and backward through the detector. A delay cable placed in the stop signal line permits both γ-rays to be timed. Data is selected from pairs of cells with 100 cm flight path. The two distinct peaks that result are seen in Fig. 6a separated by 6.3 ± 0.3 nsec, twice the transit time of the γ-rays. The minimum between the peaks corresponds to zero time.

The flight time versus channel number was determined using a pulse generator with a series of accurately known delay lines. The time resolution was determined from the width of the γ-ray

peaks and from sea level μ-mesons. As seen in Figure 6b, the half width at half maximum (HWHM) is 1.3 nsec.

The energy deposits from ground level μ-mesons were used to calibrate the detector for large energy deposits. Data from corresponding pairs of cells in S_1 and S_2 were selected. The system is equivalent to 8 μ-meson telescopes, each with a geometry factor of 40 cm^2-ster and a full opening angle of 30^o. The pulse height distribution from the upper scintillator is shown in Figure 7. The energy resolution has a HWHM of 13% at a mean μ-meson energy deposit of 28.5 MeV. Because the scintillator gives less light relatively for low energy protons than for μ-mesons, this energy deposit corresponds to a stopping proton of 41 MeV.[12]

Calibrations at higher energies were obtained by measuring the energy deposits of μ-mesons that traverse a cell through the average longer dimensions of 27.5 and 34.7 cm. These gave μ-meson energy losses of 52 and 66 MeV and stopping proton equivalent losses 63 and 80 MeV.[12]

For the overall calibration at lower energies, the detector was exposed to a beam of 15.3 MeV neutrons produced by the reaction of deuterons on tritium

$$d + t \rightarrow He^3 + n.$$

Neutrons leaving the target at about 45^o to the deuteron beam were incident on the detector. A typical matrix of E_{n_1} from time of flight, versus E_{p_1} from scintillator pulse height is shown in Figure 8. Events were selected for a pair of corresponding cells in S_1 and S_2. The density of points

on the plot determines the locus of the 15.3 MeV incident neutron line. At every point on the line the E_{n_1} obtained from time of flight are subtracted from 15.3 MeV to obtain a resultant E_{p_1}. The ordinate is labeled with both the derived values of E_{p_1} and the corresponding channel numbers.

The angle of incidence of the neutron is computed from equation 2 and the loci of equal energy and angle lines are plotted in Figure 8. The resultant energy resolution at 15.3 MeV is ± 1.7 MeV and the angular resolution is ± 15°.

The combined detector response to neutrons and μ-mesons was used to calibrate the pulse height analyser in terms of proton equivalent energy loss as shown in Figure 9. The response becomes non linear at high energy deposits because of saturation effects in the photomultipliers, which in turn are due to the considerable power loss in the adder circuit. It is also non linear below around 10 MeV because of the low relative light output from slowly moving protons in the liquid scintillator.

The neutron detector efficiency ϵ is defined as the ratio of the detector counting rate to the incident neutron flux, F,

$$\epsilon = \frac{\left[\frac{\Delta N}{\Delta t \Delta\theta \Delta E}\right]}{F}$$

where ΔN is the number of counts in a time interval Δt of 1 sec, zenith angle interval $\Delta\theta$ of 1 radian and energy interval ΔE of 1 MeV. The flux is the number of incident neutrons/cm^2-sec-ster-MeV. The efficiency is found from the equation

$$\epsilon(E,\ \theta) = N_H \cdot \left[\frac{d\sigma(E_n,\theta)}{d\Omega}\right]_{n,p} \cdot \left[N_H\sigma_{np}(E_{n_1}) + N_C\sigma_{nc}(E_{n_1})\right] \cdot$$

$$\left[f_o(E)\, f_1(E)\, V^2\ 2\pi\frac{\sin\theta}{r^2}\right]$$

where:

θ is the zenith angle of the incident neutron.

N_H is the density of hydrogen atoms in the liquid scintillator.

N_C is the density of carbon atoms in the liquid scintillator.

f_o is a factor that corrects for the attenuation of the incoming neutrons.

f_1 is a factor that corrects for the attenuation of the scattered neutrons from the first detector before they reach the second detector.

V is the volume of liquid scintillator in each cell.

r is the distance between the tanks.

$\left[\frac{d\sigma(E_n,\theta)}{d\Omega}\right]_{n,p}$ is the differential scattering cross section from hydrogen in the first detector, evaluated at E_n, that gives a signal above the threshold in S_1.

$\sigma_{np}(E_{n_1})$ is the total cross section for np scattering in the second detector, evaluated at E_{n_1}, that gives a signal above the threshold in S_2.

$\sigma_{nc}(E_{n_1})$ is the total cross section for carbon in the second detector, evaluated at E_{n_1}, that gives a signal above the threshold in S_2.

The cross sections are known to better than 5%. The factors f_o and f_1 are derived from cross section data also, and include attenuation in the gondola, anticoincidence scintillator and the tanks containing the liquid scintillator. The above equation does not include the contribution to the counting rate from neutrons that inelastically scatter from carbon in the first scintillator. This is a negligible percentage of the total number of detected events mainly because of the low conversion efficiency of energy to visible light for slowly moving heavy ions.

This detector represents a significant advance in the development of instruments designed to measure neutrons in the energy range of 2 to 100 MeV. It has applications not only to neutron measurements in the earth's atmosphere and neutrons from the sun, but in the monitoring of neutrons in ground environments as well. For example it may be useful around nuclear reactors and high energy particle accelerators.

6. ACKNOWLEDGEMENTS

We are very grateful to the Department of Defense Themis Contract No. N00014-69-A-0200-5001, the National Aeronautics and Space Administration Grant No. NGR-05-008-022, the Office of Naval Research Contract No. N00014-69-A-0200-5004, and the Air Force Weapons Laboratory Contract No. F29601-69-C-0029 for support of the design and construction of the experiment and the balloon flight to obtain the measurements. We would also like to acknowledge the significant contributions of Richard Shelton, Starnes Walker and Shin Moon to the construction and test of the detector.

REFERENCES

1) A. B. Severny, Annual Review of Astronomy and Astrophysics, 2 (1964) 363-400. A. Severny and V. Shabansky, Krymsk, Astrofiz. Obs., 25 (1961) 88.

2) W. N. Hess, Proceedings of the Fifth InterAmerican Seminar on Cosmic Rays, La Paz, Bolivia (1962) 17-27.

3) R. E. Lingenfelter, E. J. Flamm, E. H. Canfield and S. Kellman, J. Geophys. Res. 70 (1965) 4077-4095.

4) J. A. Lockwood, to be published (1972).

5) R. S. White, Bulletin, American Physical Society, Series II, Vol. 13, No. 4 (1968) 714.

6) A. M. Preszler, G. M. Simnett and R. S. White, to be published, Phys. Rev. Letters (1972).

7) D. A. Gedcke and W. J. McDonald, Nucl. Instr. and Methods, 58 (1968) 253-260.

8) R. L. Chase, Rev. Sci. Inst., Vol. 39, No. 9 (1968) 1318.

9) O. Pitzalis, Jr. and T. P. M. Couse, Proceedings of the Electronics Components Conference (1968) 207.

10) O. Pitzalis, Jr. and T. P. M. Couse, Letters, Proc. of I.E.E.E., April (1968) 738.

11) Motorola Semiconductor Prod., AN-471.

12) R. C. Webb, M. G. Hauser and R. E. Mischke, Princeton Pennsylvania Accelerator Report, PPAR 26 (1970).

FIGURE CAPTIONS

Figure 1. a) The neutron double scatter. The incident neutron n scatters from proton P_1 in the first scintillator bank and continues as on n_1 to the second scintillator bank where it scatters from proton P_2. b) A schematic section through the detector system. The two liquid scintillator tanks S_1 and S_2, the plastic anti-scintillators A_{11}, A_{13}, A_{12}, A_{21}, A_{23}, and A_{22}, the photomultipliers and the light pipes are shown.

Figure 2. The detector mounted on the lower spherical cap of the gondola. One side of the anticoincidence scintillator has been removed from the top scintillator bank to show the photomultipliers that view the individual cells of S_1. The plastic scintillators are connected by light pipes to separate photomultipliers. Semirigid 50Ω coaxial cable connects the photomultipliers to the electronics, which consists of printed circuitry mounted on a common ground plane.

Figure 3. A block diagram of the electronics system. It includes the scintillators, adders, gates, pulse height analyzers, time of flight circuit, data encoder and transmitter and ground data reduction equipment.

Figure 4. The signal adders. a) A section of the transformer configuration. b) The transmission line analogue. c) This

shows how adder sections can be cascaded to add eight signals together.

Figure 5. The time of flight circuit. The circuit uses a time to voltage to binary conversion. A voltage proportional to the time of flight is generated, held and converted to an 8-bit binary output using the double ramp conversion technique.

Figure 6. a) A time of flight spectrum for ground level cosmic ray μ mesons. b) A time of flight spectrum for γ rays from neutron induced reactions in the scintillator tanks. The separation of the peaks is 6.3 $\pm$ 0.3 nsec. The curve has been smoothed using a three point summing mean of adjacent data points.

Figure 7. A pulse height spectrum for the energy loss in one cell of S_1 for ground level cosmic ray μ mesons which had near vertical trajectories through the detection.

Figure 8. A time of flight versus pulse height matrix for 15.3 MeV neutrons. Energy and angle contours are plotted according to equations (1) and (2) (see text).

Figure 9. The calibration curve for pulse height channel number versus equivalent proton energy. The curve is based on 15.3 MeV neutron calibrations at low energies and the response to well collinated beams of cosmic ray μ mesons at the high energies.

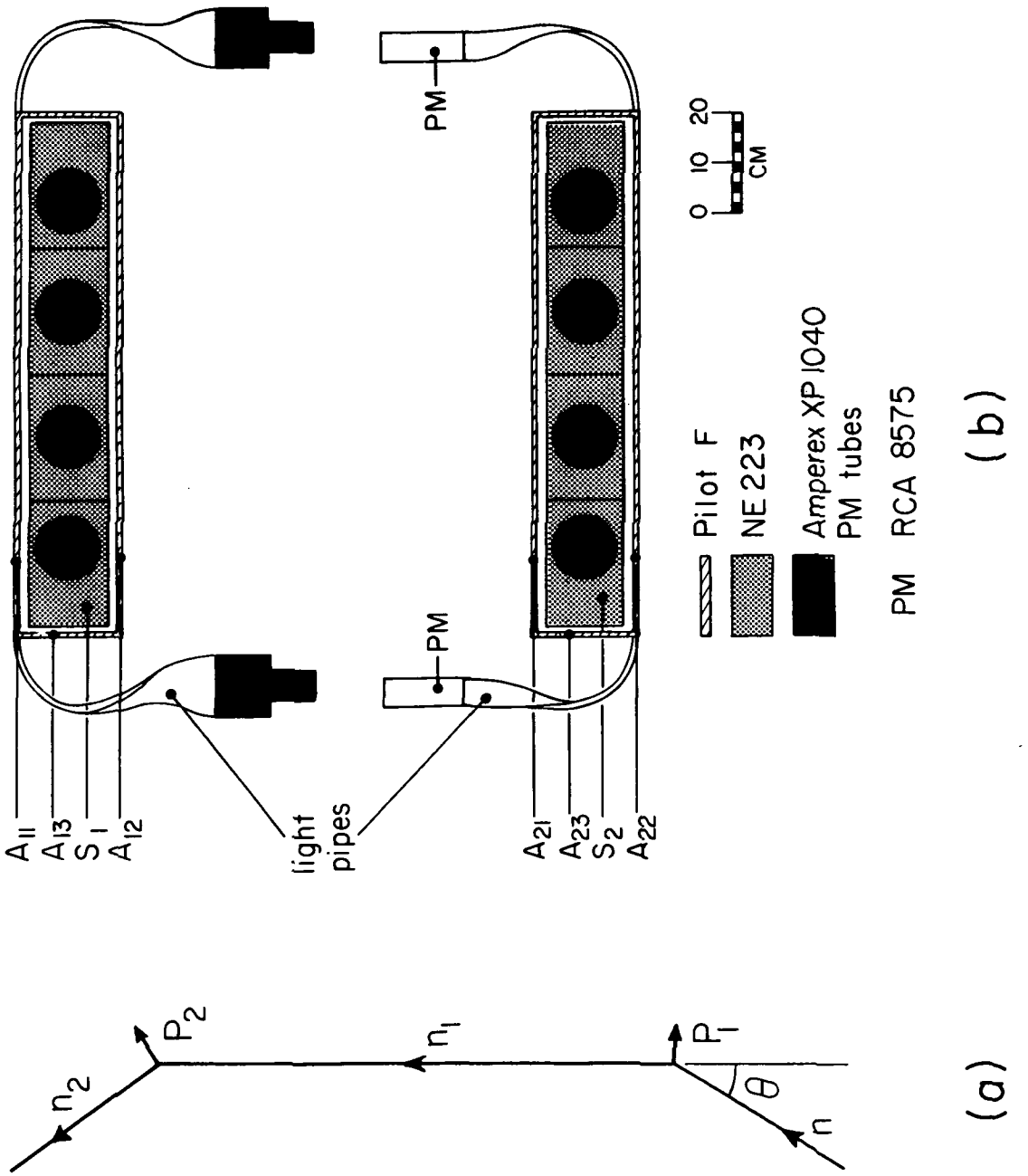
PM
PM
0 10 20
CM
Pilot F
NE 223
Amperex XP 1040
PM tubes
PM RCA 8575
(b)
A11
A13
S1
A12
light
pipes
A21
A23
S2
A22
P2
n1
P1
n2
θ
n
(a)

Figure 1

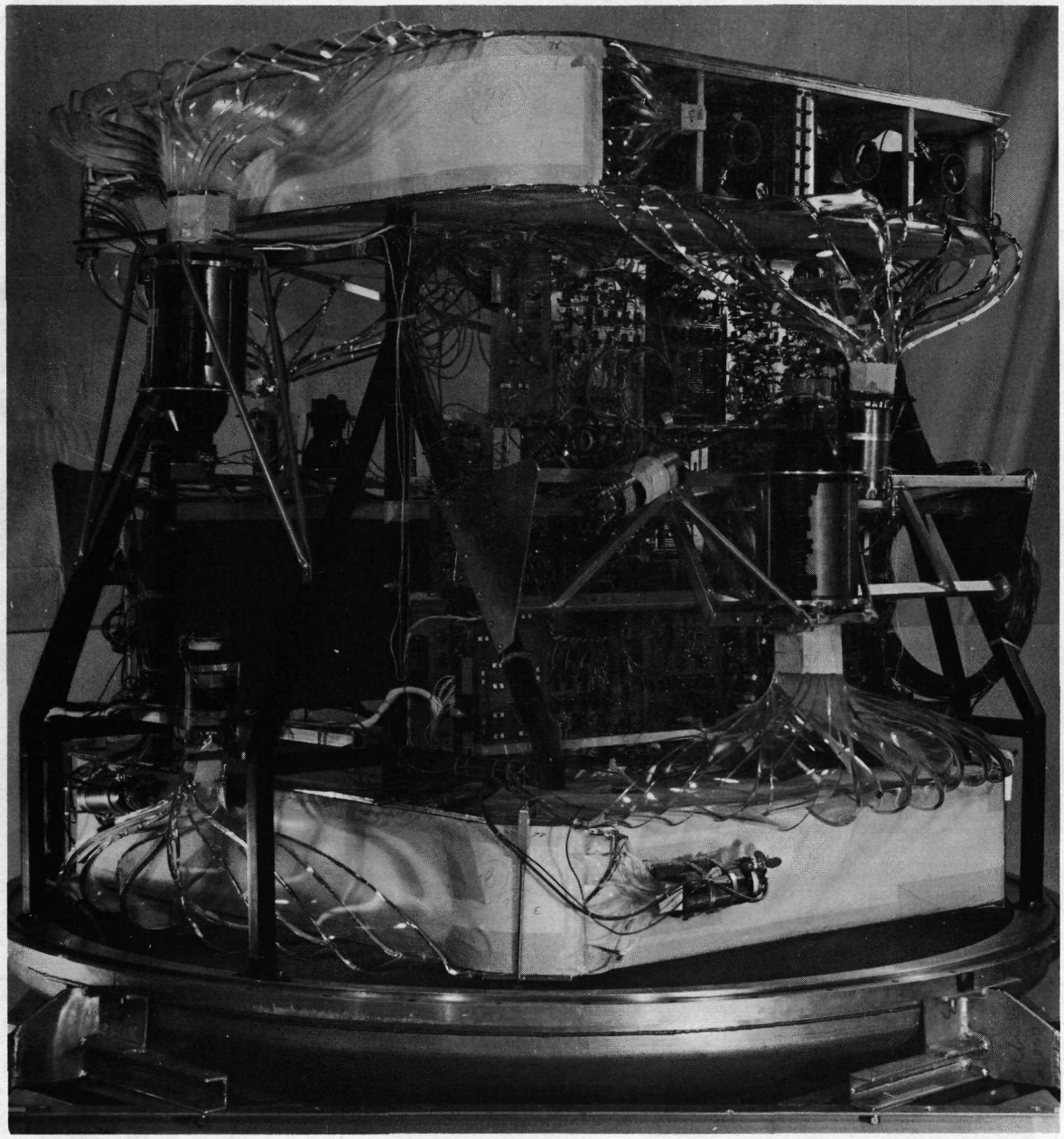

Figure 2

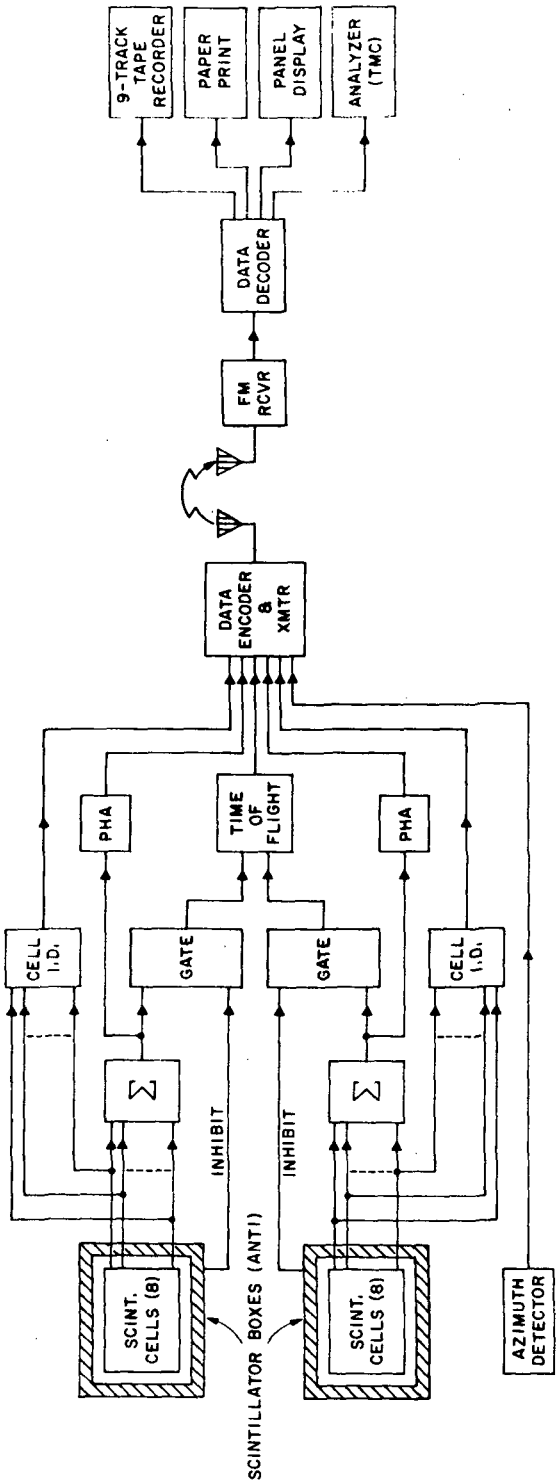
9-TRACK TAPE RECORDER
PAPER PRINT
PANEL DISPLAY
ANALYZER (TMC)
DATA DECODER
FM RCVR
DATA ENCODER & XMTR
PHA
TIME OF FLIGHT
PHA
CELL I.D.
GATE
GATE
CELL I.D.
Σ
Σ
INHIBIT
INHIBIT
SCINT. CELLS (8)
SCINT. CELLS (8)
SCINTILLATOR BOXES (ANTI)
AZIMUTH DETECTOR

Figure 3

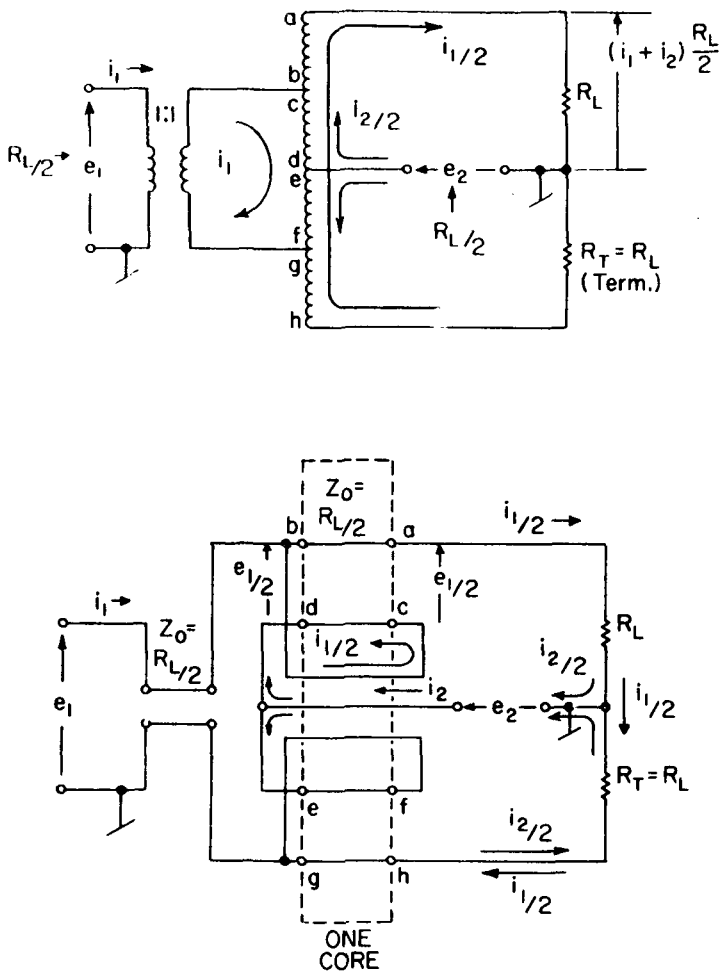
a
b
c
d
e
f
g
h
i_1
1:1
$R_{L/2}$
e_1
i_1
$i_{1/2}$
$i_{2/2}$
$(i_1 + i_2)\frac{R_L}{2}$
R_L
e_2
$R_L/2$
$R_T = R_L$
(Term.)
$Z_0 = R_{L/2}$
$e_{1/2}$
i_2
ONE CORE
Inputs from P.M. Tube Anodes
12Ω
25Ω
50Ω
PHA

Figure 4

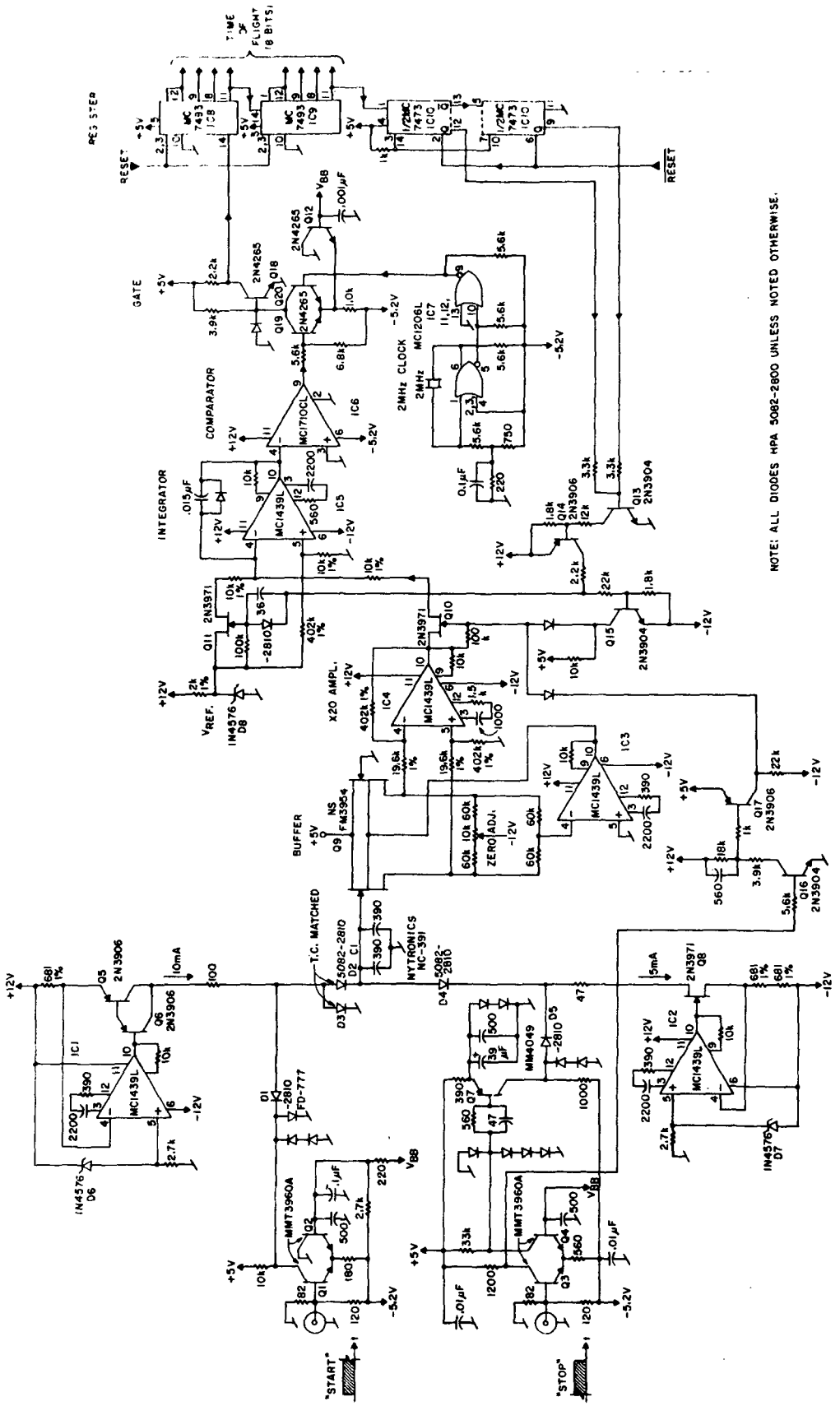
NOTE: ALL DIODES HPA 5082-2800 UNLESS NOTED OTHERWISE.
RESET
GATE
COMPARATOR
INTEGRATOR
2MHz CLOCK
X20 AMPL.
BUFFER
ZERO ADJ.
T.C. MATCHED
"START"
"STOP"

Figure 5

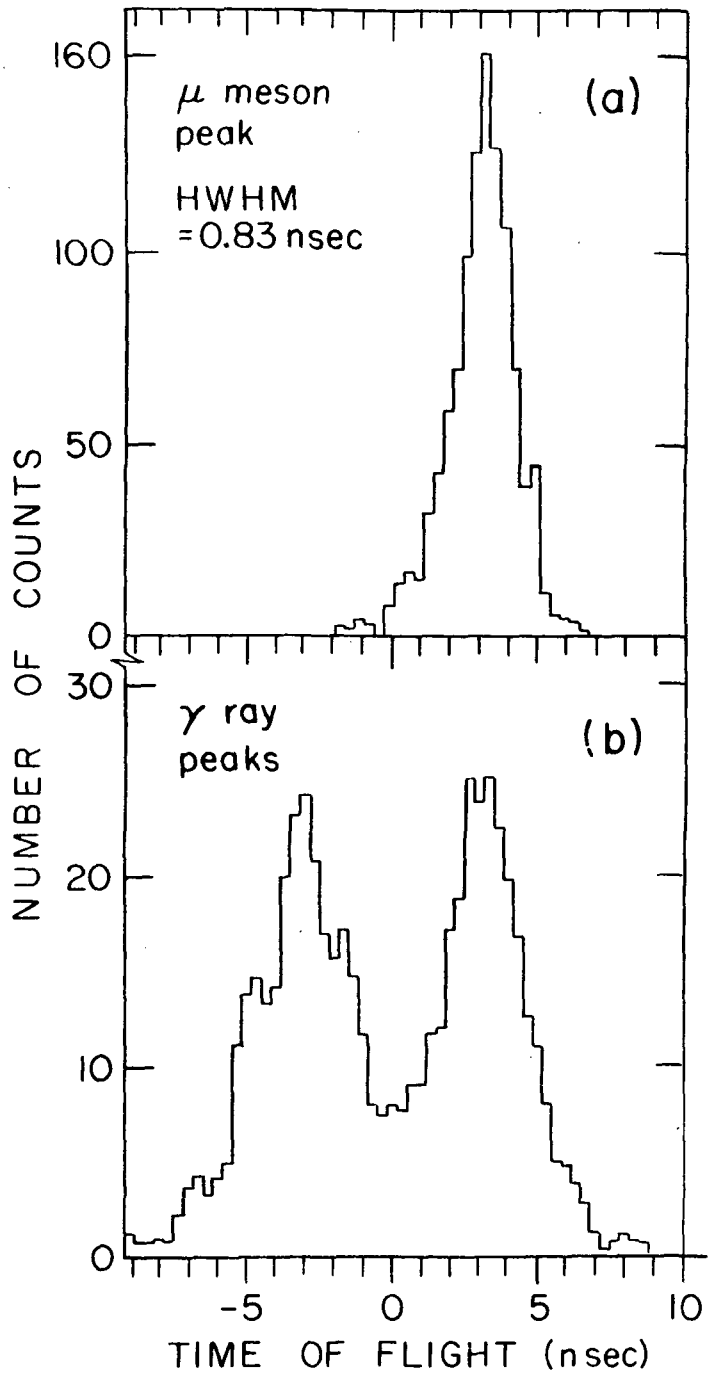
160
100
50
0
μ meson
peak
HWHM
=0.83 nsec
(a)
30
20
10
0
γ ray
peaks
(b)
NUMBER OF COUNTS
-5
0
5
10
TIME OF FLIGHT (nsec)

Figure 6

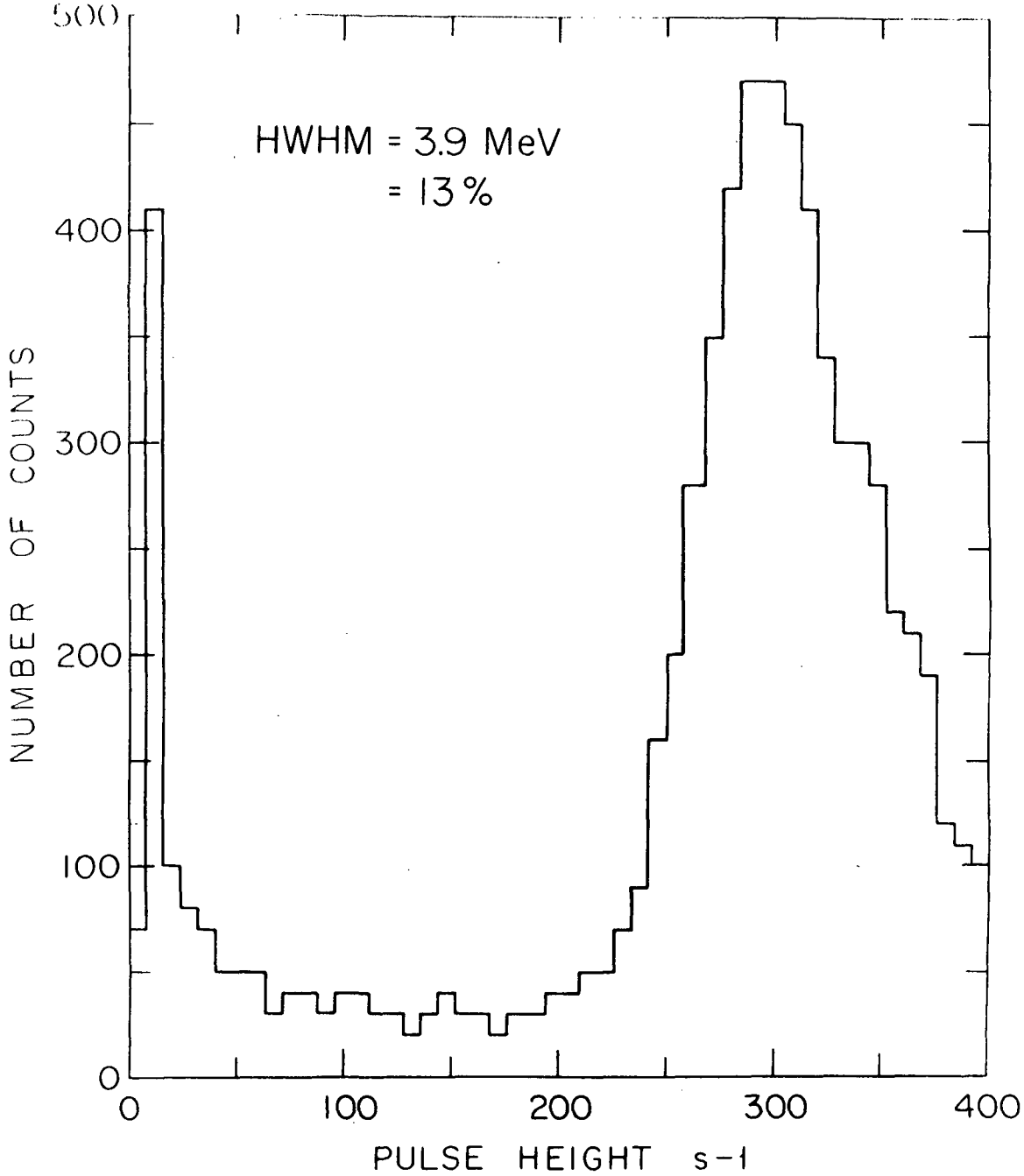
HWHM = 3.9 MeV
= 13 %
NUMBER OF COUNTS
PULSE HEIGHT s-1
0
100
200
300
400
500

Figure 7

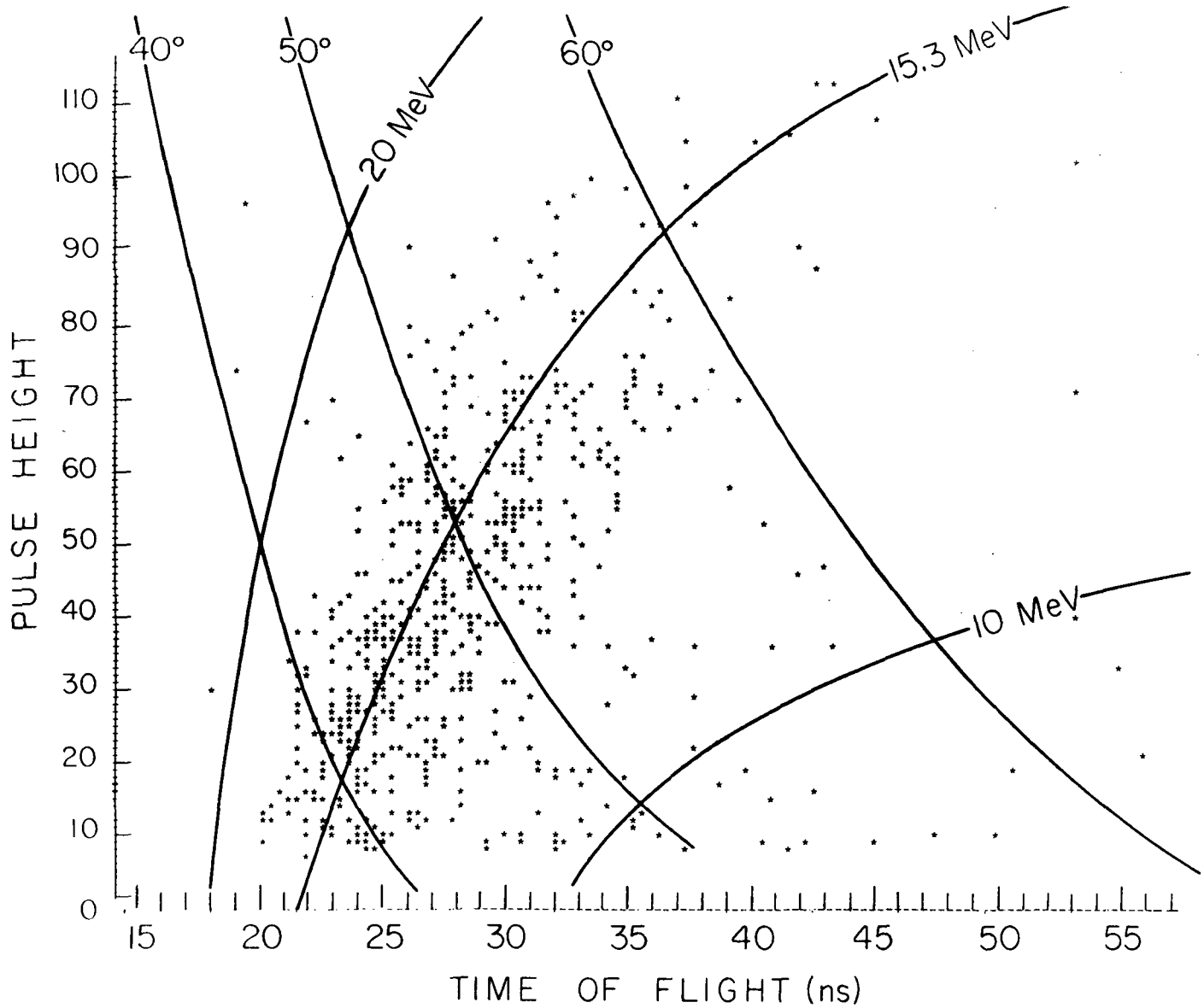
40°
50°
60°
20 MeV
15.3 MeV
10 MeV
PULSE HEIGHT
0
10
20
30
40
50
60
70
80
90
100
110
15
20
25
30
35
40
45
50
55
TIME OF FLIGHT (ns)

Figure 8

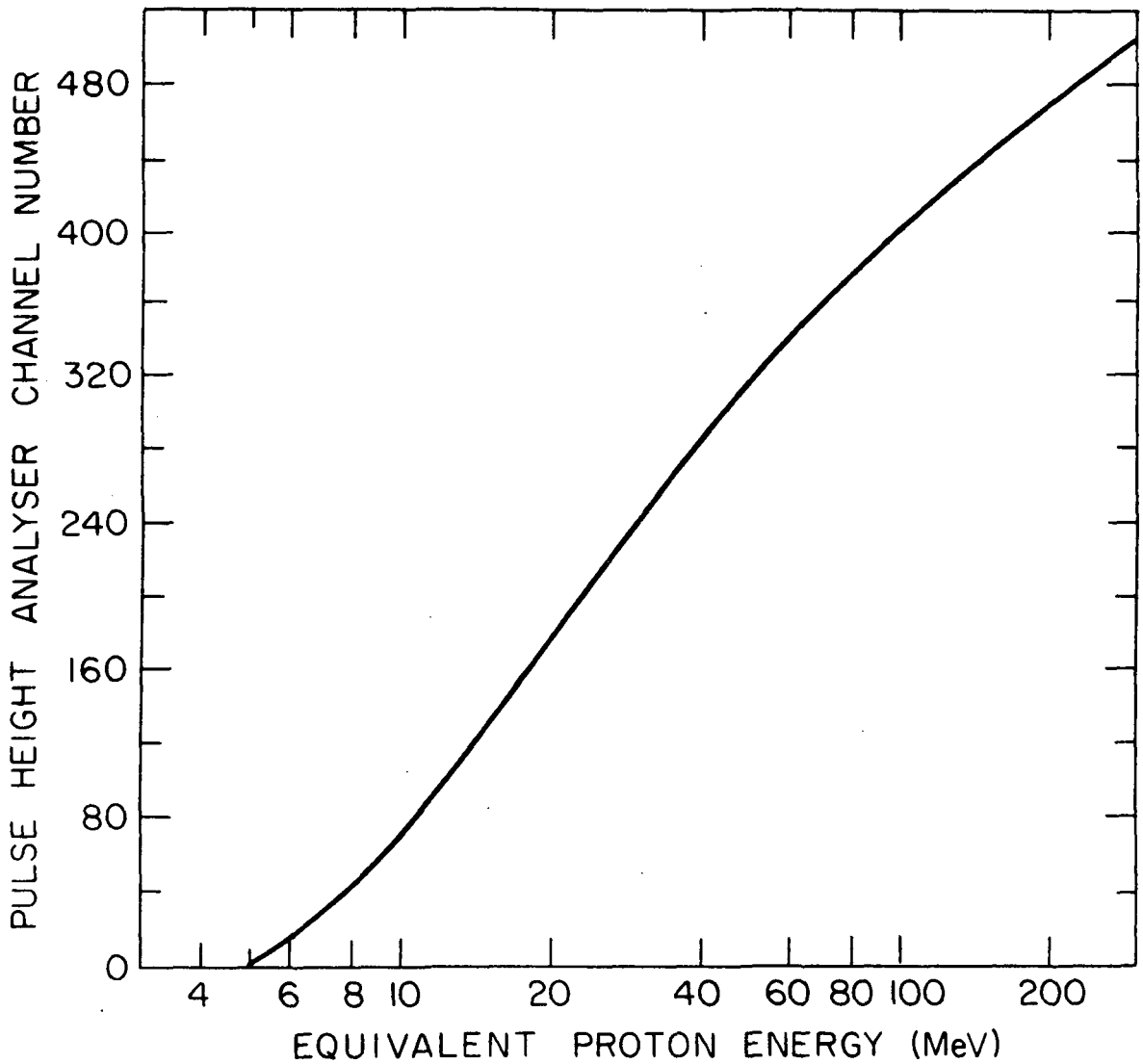
PULSE HEIGHT ANALYSER CHANNEL NUMBER
480
400
320
240
160
80
0
4
6
8
10
20
40
60
80
100
200
EQUIVALENT PROTON ENERGY (MeV)

Figure 9